OPTIMIZATION OF THE CORROSION BEHAVIOR OF MULLITE REFRACTORIES AGAINST ALKALI VAPOR VIA $ZrSiO_4$ ADDITION TO THE BINDER PHASE

M. SERHAT BAŞPINAR*, FERHAT KARA**

**Afyon Kocatepe University, Technical Education Faculty, ANS Campus 03200, Afyonkarahisar, Turkey*
***Anadolu University, Engineering Faculty, Material Science Engineering Department, 2 Eylul Campus, Eskişehir, Turkey*

E-mail: sbaspinar@aku.edu.tr

Submitted April14, 2009; accepted July 10, 2009

Keywords: Refractories, Mullite, $ZrSiO_4$, Corrosion, Alkali

Effect of $ZrSiO_4$ addition to the binder matrix of the reaction sintered mullite refractories on the alkali corrosion (Na_2CO_3, at 1370°C) behaviour was investigated. Important improvements on the corrosion behaviour were observed when zircon was introduced to the binder matrix of the mullite refractories. Zircon addition to the mullite forming mixtures improved the densification. Densification effect reduced the tendency of infiltration of the alkali vapours. The investigation of the corrosion product at the reaction interface revealed that after alkali vapour (Na_2O) attack, mullite phase decomposed into sodium-aluminate-silicate type phase (carnegieite) and alumina. These expansive phase formation is the main reason for the damage after alkali vapour attack. It was concluded that, apart from densification effect with zircon addition, mullitization and densification behaviour of the binder matrix and type of the stage grains (sinter or fused) are important factors for the alkali corrosion behaviour of the mullite refractories.

INTRODUCTION

Refractories are subjected to 3 different type of loadings; (*i*) thermal (high temperature, thermal shocks), (*ii*) mechanical (creep, walls, charges), (*iii*) chemical (high temperature corrosion of solids, liquids and gases). These loadings become more severe over the time because of the increase in the production capacity of the furnaces and higher process temperatures. Therefore, optimization of the refractories to the increased loadings is an important research area for the material science. The resistance of refractories against these loadings is determined by the properties of the stage grains, binder matrix and pore structure. Service life of refractories is usually determined by the corrosion. Individual corrosion behaviour of stage grains and binder matrix are the most important factors for the corrosion behaviour of the overall refractory system. Porosity amount and pore structure are another factors influencing the corrosion behaviour. Manufacturing of new glass types requires new glass furnace designs with higher chemical loadings and higher performance of the refractories to resist new service conditions [1, 2].

Mullite is a strong material with low thermal expansion, low thermal conductivity, excellent creep resistance, good chemical stability and high-temperature resistance that is used for advanced structural and functional applications. Although this material occurs rarely in nature, synthetic mullite is a promising candidate for most advanced refractory applications [3-8]. Mullite refractories are used in the glass melting furnaces with aggressive environment at the regenerators, ports and top structures. They are produced from sinter or fused mullite grains with different binding matrixes depending on the severity of the loads. [9-12]. One of the most severe chemical attacks on refractories in glass melting furnaces results from alkali vapours. Alkali vapours are extremely reactive and cause detrimental corrosion and control the lifetime of the refractories [13-15].

The service life of the refractories under these conditions can be improved via optimization of the stage grain, pore structure and binder matrix. Although each of these three is important, binder matrix has a special importance for the corrosion behaviour of the whole refractory system, because, it is more susceptible to corrosion than the stage grains. Thus, the improvements of the binder matrix properties are the key function for the improvement of the service lifetime. Mullite stage grains are usually bonded by reaction sintering of quartz-alumina or kaolin-alumina mixtures to obtain mullitic binder matrix in mullite refractories. Selection of binder matrix type depends on the required performance (creep, thermal shock resistance, corrosion behaviour etc.) of the refractories.

Densification is an important problem during reaction sintering of mullite. Because expansion occurs during mullite formation and the diffusion rate of Al and Si ions in mullite matrix are very low. The density of the reaction sintered mullite reaches therefore only 80-90% of the theoretical density [16, 17]. Previous studies showed that the addition of zirconia (ZrO_2) to the mullite improves the densification [18-20]. However the addition of ZrO_2 is not an economical way. The reaction sintering of zircon and alumina (Al_2O_3) mixture is more economical way to introduce zirconia into the mullite matrix according to the reaction;

$$2\ ZrSiO_4 + 3\ Al_2O_3 \rightarrow 2\ ZrO_2 + 3Al_2O_3{\cdot}2SiO_2$$

Early studies showed that reaction sintering of $ZrSiO_4/Al_2O_3$ mixture provides better distribution ZrO_2 particles and better fracture toughness values [21-23].

The aim of this work is to evaluate the alkali corrosion behaviour of mullite refractories by optimizing the binder matrix with $ZrSiO_4$ addition. Six different series of mullite refractories were produced on the basis of sinter and fused grade stage grains and three different types of binder to obtain mullitic matrix; *i*) QA (quartz/alumina), *ii*) KA(kaolin/alumina) and *iii*) KA16Z (kaolin//alumina/16% zircon). Alkali corrosion resistance of these mullite refractories was investigated.

Table 1. Grain size range and mix proportions of the stage grains.

Grain size range (mm)	Proportion (wt.%)
1-3	40
0.5-1.0	15
0-0.5	15
<0.045 (Binder phase)	30

Table 2. The composition and properties of the binder phases used for specimen preparation (Q - quartz, A - alumina, K - kaolin, Z - zircon).

Binder phase composition.	QA	KA	KA16Z
$ZrSiO_4$ (wt.%)	0	0	16
d_{50} µm	4.5	5.0	4.0
Shrinkage (%) 1700 °C	+2.3	-7.9	-9.4

EXPERIMENTAL

Material preparation and refractory properties

Test samples were prepared from different grain size fractions of fused and sinter mullite. The grain size of the stage grains and their weight percentages were given in Table 1. In KA16Z binder composition 16 wt.% of zircon was added to the KA type binder composition (see Table 2) in order to obtain following reaction equilibrium:

$$0.8(Al_2O_3{\cdot}2SiO_2{\cdot}2H_2O) + 2.2\ Al_2O_3 + 0.4\ ZrSiO_4 \rightarrow \\ \rightarrow 3Al_2O_3{\cdot}2\ SiO_2 + 0.4\ ZrO_2 + 1.6\ H_2O \qquad (1)$$

Binder mixtures were chosen on the basis of complete 3:2 mullite formation. According to the Reaction (1), the calculated amounts of raw materials were dry milled in ball mill for 6 hours to de-agglomerate the powders and increase the reaction capacity of the starting material. The particle size d_{50} (µm) after milling is given in Table 2.

The origin and chemical composition of the commercially available raw materials are specified in Table 3.

Binder matrix raw materials and mullite stage grains were mixed in Eirich type mixer. First coarse stage grains were put in to the mixer. After pouring one third of the pressing aid liquid (1 % dextrin dissolved in water: 3.5 % of the dry weight of the total solid materials), finer stage grains were added to the mixture. Finally, binder matrix was introduced to the mixture with the rest of the pressing aid liquid and mixed for 5 minutes.

Cylindrical test samples (50 mm diameter × 50 mm height) were pressed in a steel die under a pressure of at 50 MPa pressure using a hydraulic pressing machine. They were heated with the heating rate of 5°C/min and sintered at 1700°C for 4 hour. Then, 20 mm diameter holes were drilled by diamond cutting tools to obtain cup shape for corrosion testing. Additional 25×25×150 mm^3 bars were produced for the measurement of 3 point bending strength, hot modulus of rupture (HMOR) and dynamic elastic modulus. Archimedes technique was used to determine bulk density and apparent porosity of the samples. Linear thermal expansion coefficient of the samples was measured up to 1300°C. The measured physical and mechanical properties of the refractory samples are given in Table 4. The reported values were

Table 3. The suppliers and the chemical composition (wt.%) of the commercially available raw materials used for the material preparation.

	SiO_2	Al_2O_3	Fe_2O_3	CaO	MgO	TiO_2	K_2O	Na_2O	ZrO_2	LOI
Kaolin (Zettlitz)	48.2	37.2	0.6	0.15	0.3	0.06	0.9	0.1	–	12.5
Quartz, Sikron SF500	99	0.3	0.05	0.1	–	–	0.2	–	–	0.25
Alumina, Alcoa CT19FG	0.02	99.8	0.02	0.01	–	–	–	0.06	–	–
Zircon, Helmuth Kreutz Mahlwerke Gmbh.	32.05	0.6	0.1	0.35	0.05	0.1	–	–	63.3	–
Sinter, Mullite, Nabaltec Symulox M72	27.01	72.4	0.08	0.02	0.04	0.03	0.2	0.16	–	–
Fused, Mullite, Motim Edelkorund Gmbh.	23.12	76.33	0.04	0.017	–	0.015	–	0.03	–	–

obtained as an arithmetic mean value of the 5 measurements for each group of samples. It is obvious from the Table 4 that sinter mullite grains result in better properties and it also activates the sintering.

Table 4. Physical and mechanical properties of the refractory samples sintered at 1700°C.

Binder type	Q	A	K	A	KA	16Z
Grain type	Sinter (S)	Fused (F)	Sinter (S)	Fused (F)	Sinter (S)	Fused (F)
Compression strength (MPa)	68	73	104	104	119	122
Bending strength (MPa)	9.80	10.40	19.50	15.40	25.70	19
HMOR 1400°C	4.60	5.40	15.10	9.0	21.30	7.80
Dynamic elastic modulus (GPa)	35.70	26.30	71.40	47.30	83	46.10
Expansion coefficient at 1300°C	5.40	5.16	5.08	5.39	5.57	5.40
Bulk density (g/cm^3)	2.46	2.52	2.58	2.61	2.67	2.70
Apparent porosity (%)	20.90	18.90	12.40	13.60	8.90	10.10

Hot corrosion

The tests of the alkali vapour resistance of the refractory samples were done according to ASTM C987 [24]. This testing procedure is usually applied for determination of corrosion resistance of the refractories of the glass melting furnaces by using Na_2CO_3 as an alkali vapour source. The samples with 5 g Na_2CO_3 (J. T. Baker, Reagent Na_2CO_3 3602-01) in the drilled hole were heated in the muffle type laboratory furnace. Refractory plate (similar material of samples) was put on the cup shape samples to cover samples to prevent alkali vapour to escape from sample. The opening was covered by a refractory plate made from similar material as that of the sample to prevent alkali vapour escape. Furnace was heated to 1370°C and samples were hold for 2 hour at testing temperature. After each corrosion experiment, samples were cut into two pieces along the centrelines. Extend of the alkali vapour attack was evaluated visually on the cross sections. The corroded surfaces of the samples were characterized by XRD (X-ray diffractometry - Schimadzu 1700) and SEM (scanning electron microscopy - LEO 1430 VP) with EDX (energy dispersive X-ray spectroscopy).

RESULTS AND DISCUSSION

Figure 1 shows the damage at the outer surface of the test cups. Most severe damage was observed in the QA-S samples, which contain sinter mullite grains and quartz-alumina type binder matrix. QA-S sample has the maximum porosity amount of 20.9 % (Table 4). This results in excessive damage, fastest interaction and ultimate collapse of the sample (Figure 1a). Improved corrosion behaviour was observed when sinter grains were replaced by fused grains (Figure 1b). QA-F sample also cracked after the corrosion test but the damage level is considerably lower than in the case at QA-S sample. Fused grade grains are always denser and larger than sinter grade grains. Therefore, QA-F samples exhibit lower porosity (18.9 %) than the QA-S sample and better corrosion behaviour due to lower infiltration rates.

Alkali vapour corrosion is usually highly detrimental for the alumina-silicate type refractories because of expansive formations of new phases generating high stresses and cracks. Nepheline or albite is usually crystallized after the reaction of the alumina-silicate refractories with alkali sodium vapour [25, 26]. Apart from the stage grain type, binder type has also an important role for corrosion behaviour. QA type binder exhibits lower mullitization and densification potential than KA type binder. Un-reacted free quartz and alumina particles increased the ability of new phase formations. KA-S sample (Figure 1c) has better corrosion behaviour than QA-S sample. Using more reactive binder type improved the corrosion behaviour. Reaction sintering of kaolin-alumina mixture has better densification rate and mullitization potential than quartz-alumina mixtures. Porosity amount decreased to 12.4 % when KA type binder was used with the sinter type stage grains.

When fused grains were used with KA type binder, only small cracks were observed on the sample surfaces. Although KA-F samples have slightly higher porosity (13.6 %) than the KA-S samples they exhibit better corrosion resistance. This is possibly because sinter mullite grains contain more glass phase than fused mullite grains. Thus, sinter grains are more reactive than fused grains. Subsequently, sinter grains have more potential to form new reaction phases with alkali vapour. When zircon was added to the binder composition, corrosion resistance of the both sinter and fused grade samples significantly improved. Crack or deformations were not observed at all on the KA16Z-S and KA16Z-F samples (Figure 1e,f). However, KA16Z-F sample has slightly lower infiltration depth than KA16Z-S sample (Figure 2), despite higher porosity (10.1%).

It is obvious that the zircon addition improved the corrosion resistance of these materials. It also reduced the apparent porosity from 12.40 % (KA-S) to 8.90 % (KA16Z-S) by improving the densification behaviour of the binder matrix. Figure 3 shows the firing shrinkage values of the binder matrixes fired at 1700°C which contain different amount of zircon.

QA type binder has lowest ability to form mullite. It is still expanding due to mullite formation at 1700 oC. The highest shrinkage was observed in KA16Z material. SEM revealed well defined mullite crystals in the KA binder compositions; however it is very difficult to find

such crystals in QA type binder (Figure 4). Apparently, the greatest alkali vapour damage in QA-S samples results from incomplete mullitization and high porosity.

Fracture surfaces of the QA-S sample were investi. gated, in order to understand the mechanism of the damage after alkali corrosion test. Alkali vapour affected region of the samples were denser than the other zones. EDX analysis at the densification zone of the binder matrix showed that the chemical composition of the reaction zone is different than the original sample (Figure 5): Sodium, aluminium, silicon and oxygen atoms were found in the reaction zone whereas sodium was absent in the unaffected bulk. Cracks were also observed in the densified zone of the sample.

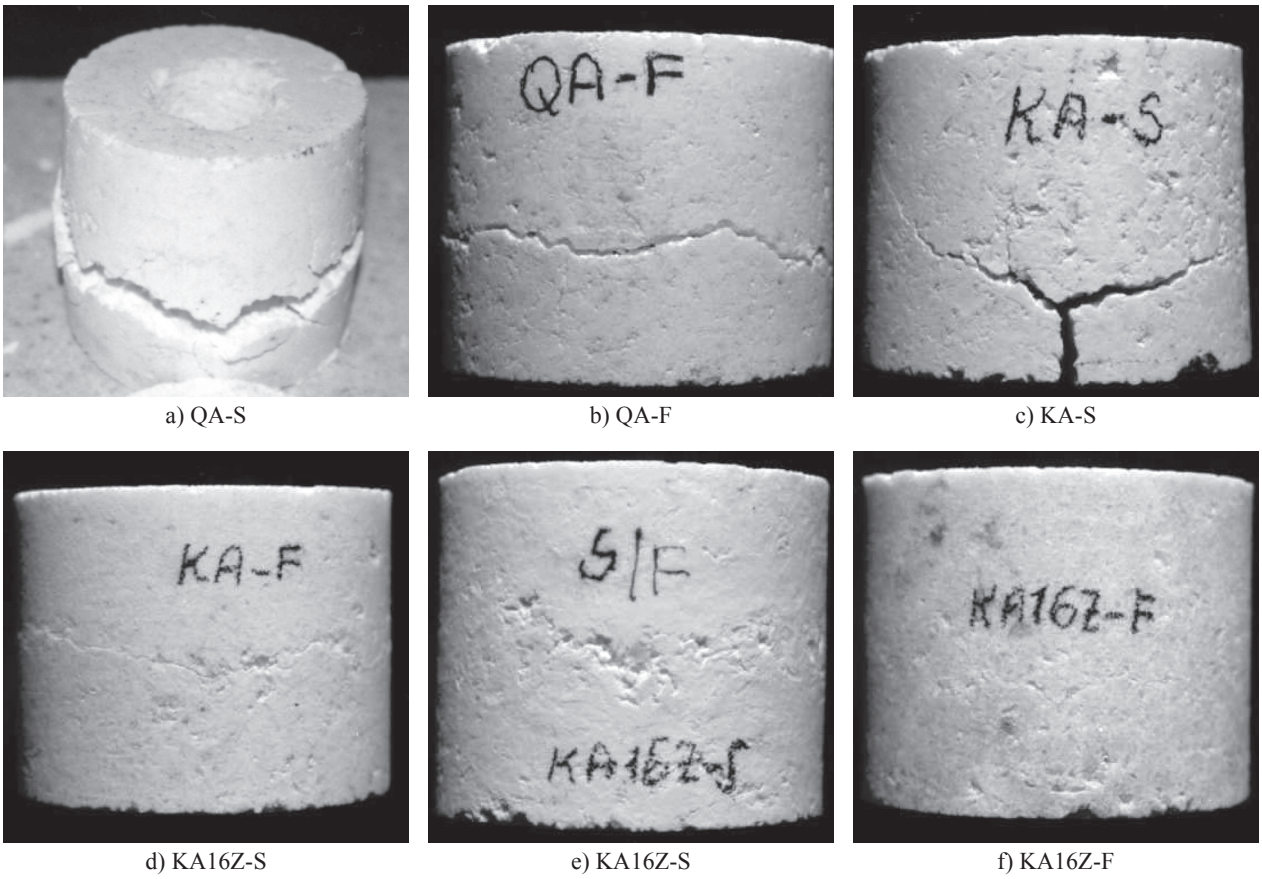

a) QA-S b) QA-F c) KA-S

d) KA16Z-S e) KA16Z-S f) KA16Z-F

Figure 1. Outer surface of the test cups after alkali attack test.

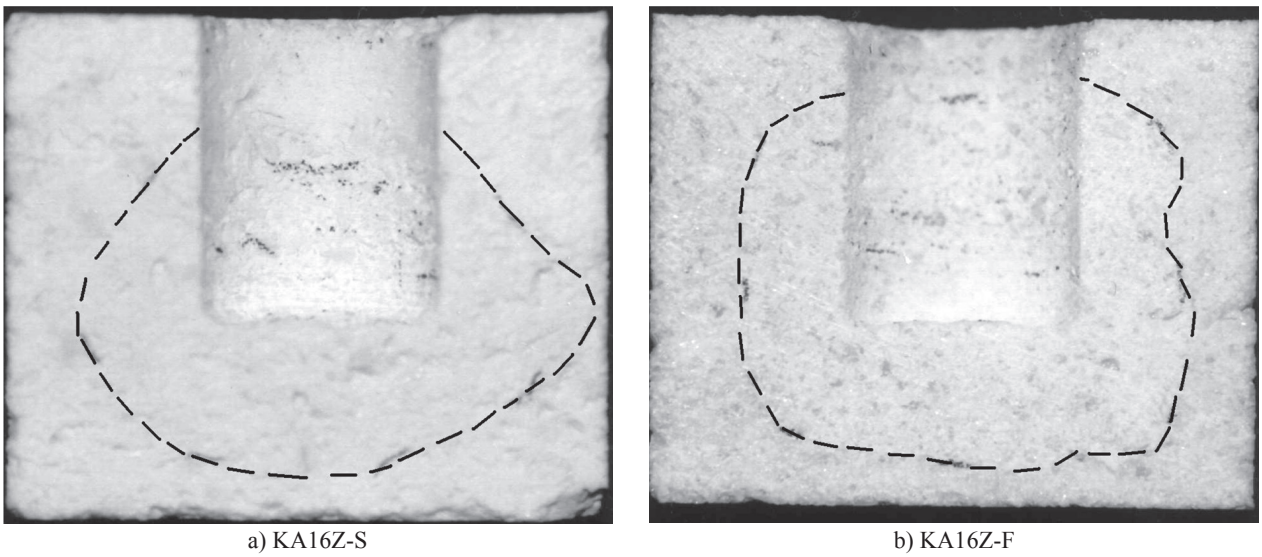

a) KA16Z-S b) KA16Z-F

Figure 2. Infiltration depth of the KA16Z-S and KA16Z-F samples.

Needle like phase formations were observed mostly in the densified zone (Figure 6) and near the cracked areas. Local EDX analysis of this needle structures found high content of aluminium with sodium, silica and oxygen as the additional elements. Needle like phases were usually attached to the locations with severely damaged areas. It seems that, they crystallized from a single point.

Alkali vapour affects binder phase and stage grains at different levels. Binder phase is more open to reactions and alkali attack causes its densification. The shrinkage of the binder phase resulted in gaps between binder phase and stage grains. It seems to be another reason for loosing of the sample integrities after corrosion test (Figure 7a).

It is very clear from the SEM pictures that, binder phase and mullite stage grains were affected in different way to alkali attack. Two different phases formed in the binder phase, sodium-aluminate-silicate type phase and needle like Al_2O_3 rich phase. Only Al_2O_3 rich phase formed on the mullite stage grain. However, the structure of the newly formed alumina rich phases on stage grain was different than at the binder matrix. It is massive, hexagonal and tabular in shape (Figure 7b).

Reaction of alumina-silicate ceramics with liquid alkalis has detrimental effect. The most deleterious is the presence of free SiO_2 and Na_2O, which increase the reaction rate at high temperatures by forming reactive glassy phases in Reaction (2).

$$2SiO_2\ (solid) + Na_2O\ (liquid) \rightarrow Na_2O{\cdot}2SiO_2\ (solid) \quad (2)$$

Alkali vapours first react with SiO_2 in the alumina-silicate type refractories When Al_2O_3 enters into the reaction, $Na_2O–SiO_2–Al_2O_3$ type phases are formed which are more refractory than $Na_2O–SiO_2$ type phases. Degree of the corrosion depends on the penetration depth of the alkali vapour through the pores [27]. Mullite which is often present in traditional chamotte refractories together with crystoballite reacts with NaO_2 above 1000°C and forms nepheline and α-alumina in reaction (3).

$$3Al_2O_3{\cdot}2SiO_2 + Na_2O \rightarrow Na_2O{\cdot} \cdot Al_2O_3{\cdot}2SiO_2 + 2Al_2O_3 \quad (3)$$

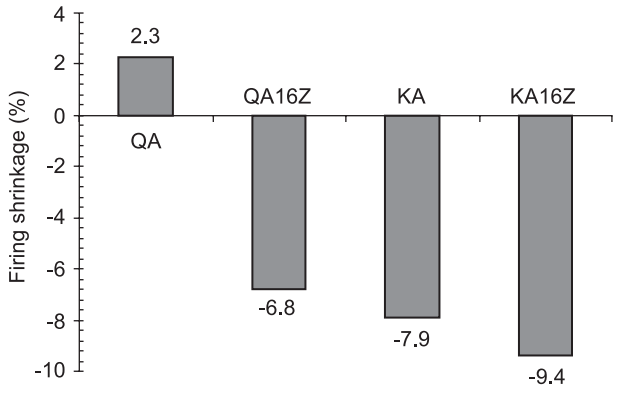

Figure 3. Firing shrinkage values of the different type mullite binders (at 1700°C). Sample size was 12×25×150 mm^3.

β-alumina ($Na_2O{\cdot}11Al_2O_3$) is formed above 1300°C [28]. As a result of the liquid alkali attack, low melting temperature phases form at the working face of the refractories. They create an impermeable layer which protects the refractory against further infiltration at low temperatures. When temperature exceeds 1260°C, glassy

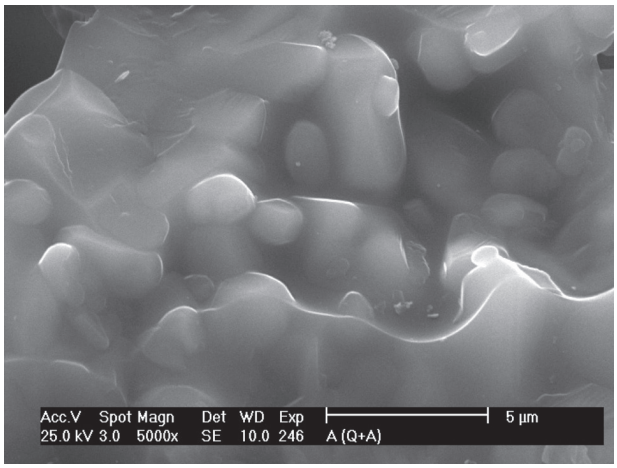

a) QA

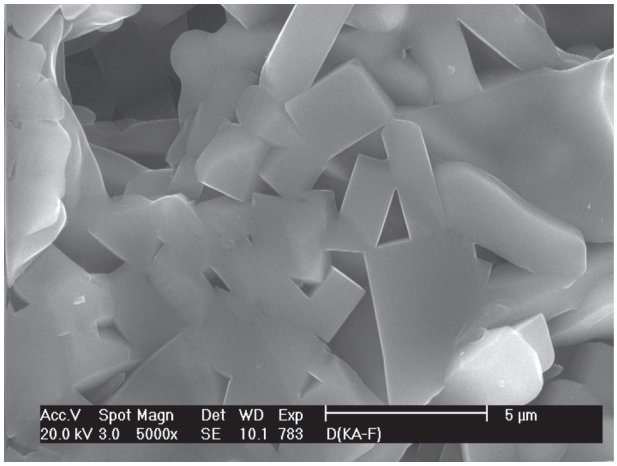

b) KA

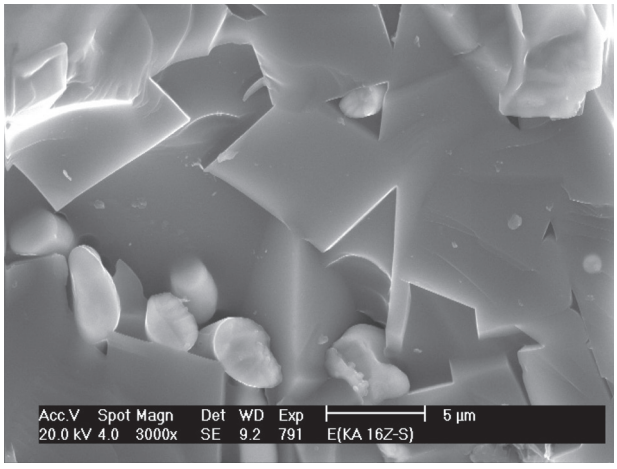

c) KA16Z

Figure 4. Microstructure differences of QA, KA and KA16Z type binders.

phases at the surfaces become more fluid and redistribute towards to colder parts of the refractory. Alkalis vaporize at increasing temperatures and penetration amount increases. Nepheline and leucite type phases are formed after the alkali attack. These phases occupy more spaces than the original refractory phases which generate internal stresses in the refractory structure. The formation of β-alumina after the reaction of Na_2O with free α-alumina is accompanied by even greater expansion and internal stresses. During cooling-heating cycles, the differences between the thermal expansions of the phases result in the accumulation of the damage in the refractory structure.

The high alumina refractories contain mullite and alumina and the reactions are different than in traditional alumina-silicates. Alumina reacts with Na_2O to form

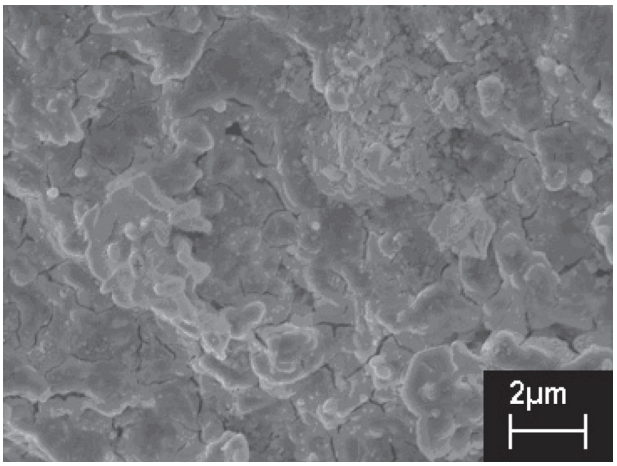

a)

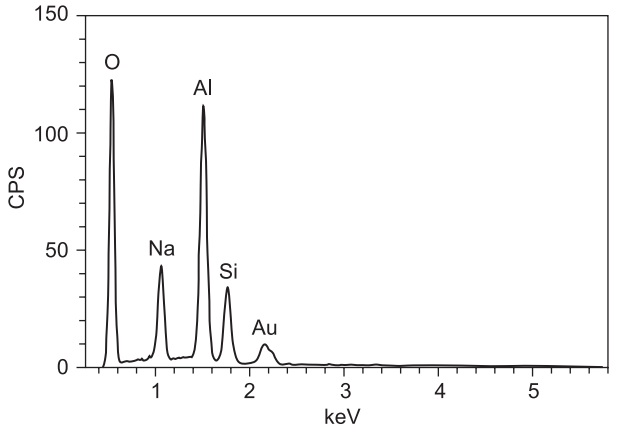

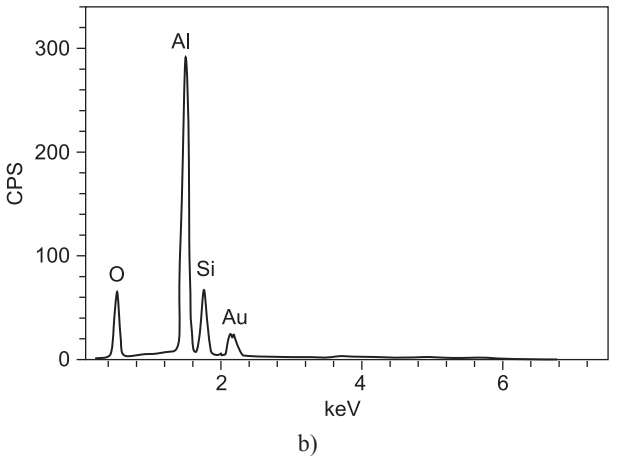

b)

Figure 5. SEM micrograph of the densified alkali vapour affected region with cracks - (a) and the composition of the EDX spectra in this zone and in the bulk of the binder matrix - (b).

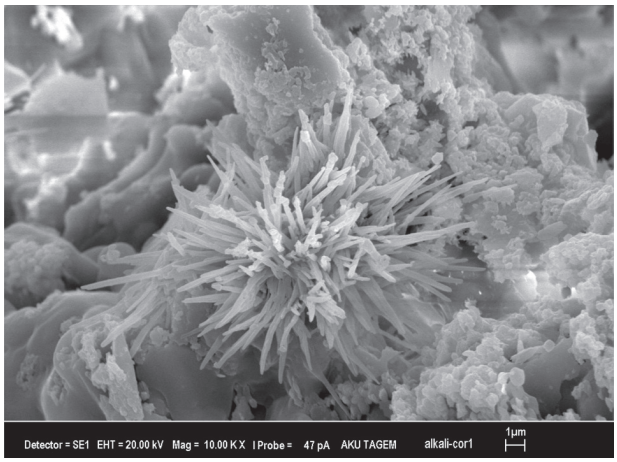

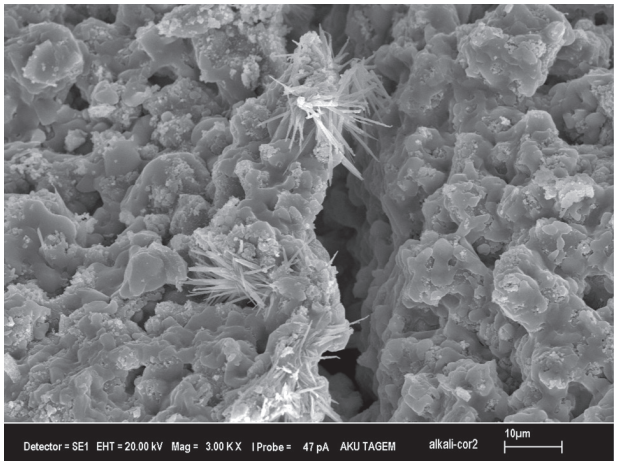

Figure 6. Needle like phase formations along the cracked areas.

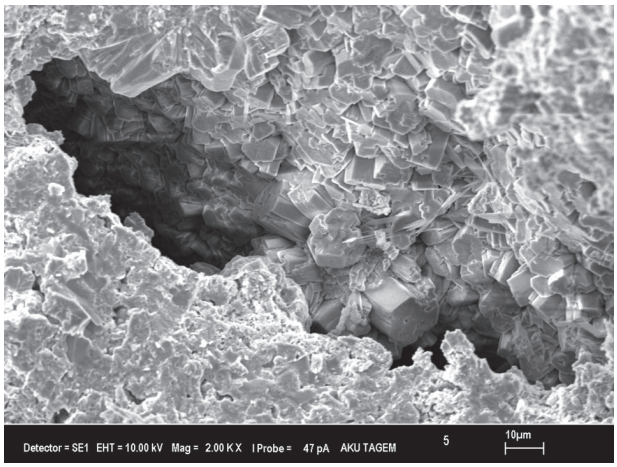

Figure 7. Binder phase-sinter mullite grain interface after alkali attack.

β-alumina. Mullite reacts with Na_2O and forms nepheline and α-Al_2O_3 up to 1250°C. Nepheline transforms to carnegieite at temperatures above 1250°C [28-31]. The presence of carnegieite was confirmed by XRD analysis in the most severely damaged zones of QA-S sample after corrosion test.

XRD analysis was done on the most severely damaged. Sample refractory pieces were taken from damaged parts of the sample. XRD analysis showed that carnegieite is formed after the reaction of mullite refractory with Na_2O vapour (Figure 8). Since mullite grains were also ground with binder matrix, mullite peaks were also observed in the XRD pattern.

QA type binder contains free Al_2O_3 due to the low mullitization rate of the quartz-alumina mixture. Reaction between free Al_2O_3 and Na_2O resulted in large stresses due to the new phase formation in most porous QA-S sample (20.9 % porosity). Increase in the expansive phase formations with increasing amount of free alumina during alkali corrosion in the refractory structure was also reported [31]. Although KA-S sample exhibits lower porosity (12.4 %) large cracked areas were also observed after corrosion test (Figure 1c). This suggests that there are other factors than porosity that affect the corrosion damage. It is well known that, sinter mullite grains are more reactive than fused mullite grains due to their higher glassy phase content. Therefore, higher glassy phase content of the sinter mullite grains increases the reaction of the mullite grains with alkali vapours. Secondly, sinter mullite grains usually contain free alumina in their phase structure. These two factors increase the extent of damage after alkali vapour attack in sinter mullite type samples.

CONCLUSIONS

Addition of zircon ($ZrSiO_4$) to the reaction sintered mullite binder matrix improves mechanical and corrosion properties of the mullite refractories. The main reason for the improvements is the densification of the mullite with zircon addition. Samples which are made from fused mullite grains have better alkali corrosion resistance than sinter mullite grain. Porosity is the main factor which controls the degree of damage after alkali vapour corrosion. Thus, infiltration depth of the alkali vapour increases with increase in porosity of the sample. Quartz-alumina (QA) type binder, which exhibits low mullitization and poor densification behaviour, has weak alkali corrosion resistance than kaolin-alumina (KA) type binder with higher mullitization and densification ability. Addition of zircon to KA type binder combined with the fused grains resulted in the best alkali corrosion resistance.

Mullite decomposition due to the reaction with Na_2O generates new phases. These expansive phases are the main reason for the damage after alkali corrosion test. Carnegieite phase was found in the reaction zone of the QA-S type mullite refractory sample. SEM and EDS investigations showed that apart from new sodium–aluminate–silicate phase formation, alumina also crystallized during alkali attack on the mullite stage grains. Reactivity of the stage grains influences the alkali corrosion behaviour of the mullite refractories.

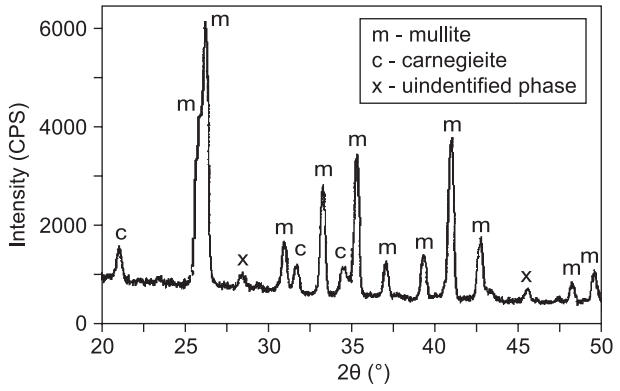

Figure 8. XRD analysis of the reaction zone of QA-S sample after alkali attack.

Acknowledgement

The authors thank DAAD (Deutscher Akademischer Austausch Dienst) for the financial support for the study and Prof. Dr. Wolfgang Schulle (TU-Freiberg IKGB) for his great support of this work.

References

1. Evans G., Baxendale S.: British Ceramic Transaction *100*, 90 (2001).
2. Evans G., Baxendale S., Deighton A.: British Ceramic Transaction *100*, 43 (2001).
3. Schneider H., Okada K., Pask J.: *Mullite and Mullite Ceramics*, Wiley, London 1994.
4. Chesters J. H.: *Refractories: Production and Properties*, The Iron and Steel Institute, London 1973.
5. Mazdiyasni K. S., Brown L. M.: J. Am. Ceram. Soc. *55*, 548 (1972).
6. Tamari N., Kondoh I., Tanaka T., Katsuki H.: J. Ceram. Soc. Jpn. 101, 721 (1993).
7. Schneider H., Schreuer J., Hildmann B.: Journal of the European Ceramic Society *28*, 329 (2008).
8. Moore R.E., Skoog A.J.: Ceramic Bulletin. 67, 1180 (1988).
9. Pick A. N. in: International Symposium on Refractories p.299-303 Hangzhou-China, November 15-18, 1988.
10. Emblem H. G., Davies T. J, Harabi A., Sargeant G. K. in: XXXV. International Colloquium on Refractories, p.170-174, 1-2 Oct, Aachen-Germany 1992
11. Davies T. J., Emblem H. G., Sargeant G. K. in: Euro Ceramics II Proceeding of Second European Ceramic Society Conference, p.2587-2591, Ed. Ziegler G. and Hausner H., 1991.

12. Amutha D. R., Gnanam F. D.: Ceramic International *26*, 347 (2000).
13. Beerkens R. G. C., Verheijen O. S.: Physics and Chemistry of Glasses - European Journal of Glass Science and Technology Part *B 46*, 583 (2005).
14. Kennedy C. R.: Journal of Materials for Energy Systems *3*, 27 (1981).
15. Kashcheev I. D., Mamykin P. S., Bartushka M.: Refractories and Industrial Ceramics *16*, 702 (1975).
16. Rezaie H.R., Rainforth W.M., Lee W.E.: British Ceramic Transactions. 96, 181 (1997).
17. Montanaro L., Perrot C., Negro A.: J. Am. Ceram. Soc. *83*, 189 (2000).
18. Lathabai S., Hay D. G., Wagner F., Clausen N.: J. Am. Ceram. Soc. *79*, 248 (1996).
19. Koyama T., Hasayhi S., Yasumori A., Okada K.: Journal of the European Ceramic Society *14*, 295 (1994).
20. Prochazka S., Wallace J. S., Claussen N.: J. Am. Ceram. Soc. *66*, 125 (1983).
21. Anseau M. R., Leblud C., Cambier F.: Journal of Materials Science Letters. *2*, 366 (1983).
22. Claussen N., Jahn J.: J. Am. Ceram. Soc. *63*, 228 (1980).
23. Zhao S., Huang Y., Wang C., Huang X., Guo J.: Materials Letter. *57*, 1716 (2003).
24. ASTM C987 - 00a (2005) Standard Practice for Vapour Attack on Refractories for Furnace Superstructures.
25. High alumina brick selection for rotary kilns, The Resco Line-A Newsletter for the Cement and Lime Industry, *3*, April (2002).
26. Interpreting refractory wear in rotary kilns, The Resco Line-A Newsletter for the Cement and Lime Industry, 2, September (2001).
27. Farris R. E., Allen J. E.: Iron Steel Engineering. *50*, 67 (1973).
28. Jacobson N. S., Lee K. N., Yoshio T.: J. Am. Ceram. Soc. *79*, 2161 (1996).
29. Velez M., Smith R.E., Moore R. E., Ceramica *42*, 283 (1997).
30. Takahashi J., Kawai Y., Shimada S.: J. Am. Ceram. Soc. *22*, 1959 (2002).
31. Rezaie A., Headrick W. L., Moore W. G., Davis W. A: Refractories Applications and News. *9*, 26 (2004).